

1 Nanopore amplicon sequencing reveals molecular convergence and local adaptation of opsin
2 genes

3 **Authors:**

4 Katherine M. Eaton^{1,2}, Moisés A. Bernal^{1,2}, Nathan J.C. Backenstose¹, and Trevor J.
5 Krabbenhoft³

6

7 ¹Department of Biological Sciences, University at Buffalo, Buffalo, NY

8 ²Current address: Department of Biological Sciences, Auburn University, Auburn, AL

9 ³Department of Biological Sciences and RENEW Institute, University at Buffalo, Buffalo, NY

10

11 Keywords: Genomics, genotyping, nanopore, long-read sequencing, parallel evolution, vision.

12

13 Corresponding author: Trevor Krabbenhoft, tkrabben@buffalo.edu

14

15

16 **Abstract:**

17 Local adaptation can drive diversification of closely related species across environmental
18 gradients and promote convergence of distantly related taxa that experience similar conditions.
19 We examined a potential case of adaptation to novel visual environments in a species flock
20 (Great Lakes salmonids, genus *Coregonus*) using a new amplicon genotyping protocol on the
21 Oxford Nanopore Flongle. Five visual opsin genes were amplified for individuals of *C. artedi*, *C.*
22 *hoyi*, *C. kiyi*, and *C. zenithicus*. Comparisons revealed species-specific differences in the coding
23 sequence of *rhodopsin* (Tyr261Phe substitution), suggesting local adaptation by *C. kiyi* to the
24 blue-shifted depths of Lake Superior. Parallel evolution and “toggling” at this amino acid residue
25 has occurred several times across the fish tree of life, resulting in identical changes to the visual
26 systems of distantly related taxa across replicated environmental gradients. Our results suggest
27 that ecological differences and local adaptation to distinct visual environments are strong drivers
28 of both evolutionary parallelism and diversification.

29

30 **Introduction:**

31 Local adaptation to novel environments presents a mechanism that can drive genetic and
32 phenotypic differentiation among closely related organisms. Diversification may occur as
33 populations become locally adapted to distinct conditions, leading to the divergence of traits that
34 are beneficial in each lineage's preferred environment. Conversely, a trait may be sufficiently
35 advantageous in a particular environment that multiple distantly related taxa converge upon it, in
36 some cases due to the same mutation or amino acid substitution occurring independently, i.e.,
37 parallel evolution (Zhang and Kumar 1997, Futuyma and Kirkpatrick 2017). For example,
38 parallel substitutions have occurred in myoglobin in pinnipeds and cetaceans (Romero-Herrera et
39 al. 1978), lysozyme in ruminants and colobine monkeys (Stewart et al. 1987) and rhodopsin in
40 fishes colonizing brackish or freshwater ecosystems (Hill et al. 2019). In this study, we examined
41 a specific case of local adaptation in the teleost visual system that has led to diversification
42 among similar taxa and parallel evolution among distantly related fishes.

43 Due to their importance in ecological interactions and their dynamic evolutionary history,
44 the evolution of visual pigment genes (i.e. opsins) in marine and freshwater fishes has received
45 considerable attention. The vertebrate visual opsin system is divided into five subgroups – one
46 rod opsin responsible for vision under low light conditions (*rhodopsin*) and four cone opsins
47 responsible for color vision (*long-wave sensitive*, *short-wave sensitive 1*, *short-wave sensitive 2*,
48 and *rhodopsin 2*) which are differentiated based on their peak absorbance spectra (Okano et al.
49 1992). Previous studies have identified two primary mechanisms through which opsin genes can
50 shape the evolution of vision: (1) Single nucleotide polymorphisms (SNPs) causing non-
51 synonymous substitutions in key spectral tuning residues driving adaptation to different light
52 environments (Terai et al. 2002, Marques et al. 2017), and (2) Copy number variation (CNVs) of

53 opsin genes with different spectral tuning (e.g., rod opsin copy number expansions in deep-sea
54 fishes [Musilova et al. 2019], and expansions of cone opsin families in shallow-water fishes
55 [Weadick and Chang 2007]).

56 The cisco species flock (genus *Coregonus*) of the Laurentian Great Lakes present a well-
57 suited opportunity to study local adaptation of the visual opsin repertoire to novel photic
58 environments based on depth differences (Harrington et al. 2015). The four extant cisco species
59 in Lake Superior show generally low levels of interspecific variation across the genome
60 (Turgeon and Bernatchez 2003, Turgeon et al. 2016, Ackiss et al. 2020) despite considerable
61 differences in depth preferences (Eshenroder et al. 2016, Rosinski et al. 2020). *C. artedi* is
62 typically epilimnetic (10-80 m), *C. hoyi* and *C. zenithicus* are both found at intermediate depths
63 (40-160 m), and *C. kiyi* can be found at depths of 80 to >200 m (Eshenroder et al. 2016). Despite
64 the overall weak genetic divergence among species of the complex, we hypothesized that
65 divergent selection may act to tune opsins to maximally absorb wavelengths of light that
66 penetrate to each species' preferred depth allowing for prey capture and predator avoidance,
67 leading to measurable genetic differentiation in these species' opsin genes. Here we assess the
68 evolution of five visual opsins in the *Coregonus* species flock to better understand mechanisms
69 underlying their evolution across a depth gradient. Our aim was to explore both local adaptation
70 to different photic conditions among the closely related *Coregonus* species, and to determine if
71 parallel changes at key spectral tuning sites have occurred among our *Coregonus* species and
72 more distantly related fish taxa.

73 **New Approaches:**

74 Oxford Nanopore sequencing is contributing to a rapidly expanding toolkit for DNA
75 sequencing, owing to low up-front costs, enhanced ability to detect DNA or RNA base

76 modifications, and read lengths limited only by input nucleic acids. Nanopore sequencing allows
77 for straightforward haplotyping, as whole molecules can be sequenced for each amplicon with no
78 need for assembly. This approach has been successfully applied to microbial metabarcoding and
79 pathogen identification (Shin et al. 2016, Moon et al. 2018, Rames and Macdonald 2018), as well
80 as human genotyping (Cornelis et al. 2017, Cornelis et al. 2019). As flow cell quality and base-
81 calling algorithms have improved, the accuracy and functionality of nanopore amplicon
82 sequencing have rapidly expanded. Yet, its application to single nucleotide polymorphism (SNP)
83 genotyping in non-human eukaryotes with large and complex genomes remains relatively
84 unexplored. In particular, a key open question is whether accurate genotypes can be obtained and
85 the coverage depth needed to do so.

86 In the present study, we sequenced amplicons of five teleost opsin genes in a total of 80
87 samples on the Oxford Nanopore Flongle device. In combination with the PCR Barcoding
88 Expansion 1-12 (Oxford Nanopore Technologies), we sequenced and genotyped 12 individuals
89 simultaneously on a single Flongle flow cell, following the pipeline shown in Figure 1 (for a
90 complete protocol, see Supplementary File S1). To the best of our knowledge, the present study
91 is one of the first to demonstrate the accuracy and utility of amplicon sequencing with the Oxford
92 Nanopore Flongle for SNP genotyping eukaryotic samples.

93 **Results and Discussion:**

94 A preliminary assembly of the de novo transcriptome of *Coregonus artedi* (NCBI
95 Bioproject XXXXX) was used as a reference to extract gene sequences of: *long-wave sensitive*
96 (*LWS*), *short-wave sensitive 1* (*SWS1*), *short-wave sensitive 2* (*SWS2*), *rhodopsin* (*RH1*), and
97 *rhodopsin 2* (*RH2*), representing one gene from each teleost opsin subfamily. For each of the five
98 genes of interest, a fragment approximately 700-2100 bp in length was amplified for 18 samples

99 of *C. artedi*, 19 *C. hoyi*, 21 *C. kiyi*, and 16 *C. zenithicus* (Tables 1, S1, S2). All amplicons from a
100 single individual were assigned a specific barcode and were pooled into a library containing
101 genes from 12 samples, which were sequenced simultaneously on a single Flongle flow cell
102 (Figure 1). This process was then repeated until amplicons from all samples were sequenced.
103 After sequencing, sample-specific barcodes were detected and trimmed using Guppy v3.2.4
104 (Oxford Nanopore Technologies) with the command *guppy_barcoder*, and reads from each
105 sample were mapped with BWA v0.7.17 using the command *bwa mem* (Li 2013), with version
106 one of the *Coregonus sp. "balchen"* genome assembly as a reference (De-Kayne et al. 2020;
107 GCA_902810595.1). An annotated bash script detailing the entire bioinformatic pipeline is
108 available from Github (<https://github.com/KrabbenhoftLab/rhodopsin>).

109 On average, Flongle sequencing runs yielded a total of 206.13 Mb (± 166.64 Mb; 26.84-
110 471.50 Mb), with an average of 184,958 reads ($\pm 154,877$ reads; 23,468-435,138 reads), though
111 yield varied based on flow cell quality (flow cells used were early release and had low starting
112 pore counts). The average sequence N50 was 1,117 bp (± 305 bp; 897-1,852 bp), with read length
113 abundances peaking at the approximate lengths of our amplicons (Figure 1). After resequencing
114 genes with low coverage following first-round sequencing, the average coverage was 3,199.58x
115 across all five genes ($\pm 4,804.24$ x, 10.47-31,158.31x; Table 1). Coverage varied slightly by
116 species, but this is likely an artifact of stochastic differences in PCR efficiency and sequencing
117 yield (Table S3). Amplicon reads mapped uniquely (i.e., one genomic region per amplicon) to
118 the *C. sp. "balchen"* genome, providing no evidence for CNVs in opsin genes among *Coregonus*
119 species.

120 To verify the accuracy of nanopore amplicon genotyping, we performed a rarefaction
121 analysis in which SNPs were called at various levels of coverage (i.e., maximum, 2,000, 1,000,

122 500, 250, 100, 75, 50, and 25x) in BCFtools v1.9 using the command *bcftools mpileup* (Li 2010,
123 Li 2011, Danecek et al. 2014). The option *-d* was used to specify the maximum per-sample
124 depth. The SNP calls from nanopore data were then compared with Sanger sequences of
125 *rhodopsin* for the same individuals. While accuracy remained high at all sequencing depths
126 (>90%), we found incongruencies in a small proportion of samples between 10x and 75x. Only
127 when reaching 100x coverage were genotypes called with complete accuracy for all individuals,
128 in relation to Sanger sequences. Considering that small errors can impact the results of analyses
129 involving amplicons with few variant sites, we recommend a minimum per-amplicon coverage
130 of 100x for future work.

131 The genotyping approach used in this study was conservative, as the goal was to assess
132 the coverage needed for accurate genotyping on a Flongle flow cell. Based on our findings, this
133 approach could be used for higher throughput sequencing, which could involve more amplicons,
134 more individuals, or a combination of both. Considering that we generated approximately 200
135 Mb of sequence data per run, one can calculate the number of individuals and amplicons that can
136 be sequenced simultaneously at 100x using the following formula:

$$200,000,000 \text{ bp} = 100 * A * N * N_A$$

137 Where *A* is the amplicon size (in bp), *N* is the number of samples to be sequenced
138 simultaneously, and *N_A* is the number of amplicons to be sequenced per sample. To optimize
139 throughput for the maximum number of samples, the PCR Barcoding Expansion 1-96 (EXP-
140 PBC096, Oxford Nanopore Technologies) can be employed to generate sequence data for 96
141 samples simultaneously. Assuming an average amplicon size of 1,000 bp, one could sequence 20
142 amplicons across 96 samples in a single 24-hour Flongle sequencing run for approximately \$300,
143 or \$0.16 per genotype (Table S4). The use of a MinION flow cell (not analyzed here) would

144 increase output by a factor of ~16x (based on differences in number of total pores) and reduce
145 the cost per genotype overall. With the growth of nanopore sequencing, these conservative cost
146 estimates are expected to drop in upcoming years.

147 The average F_{ST} of SNPs in the five opsins analyzed across four species was 0.055 (Table
148 2). The only large differences ($F_{ST} > 0.4$) were found in four SNPs detected within the coding
149 sequence of *rhodopsin*, with no highly differentiated SNPs among the four cone opsins. This
150 suggests that differences in dim-light vision and changes in *rhodopsin* could be driving local
151 adaptation by depth. Of the four high F_{ST} SNPs, one ($F_{ST} = 0.44$) was synonymous. One SNP
152 ($F_{ST} = 0.44$) resulted in a shift from asparagine to histidine at amino acid residue 100, which is
153 located near the C-terminal end of transmembrane helix two, possibly in the extracellular matrix
154 (Figures 2a, 2b; see also Yokoyama 2000). Another ($F_{ST} = 0.44$) resulted in a change from valine
155 to isoleucine at residue 255, which is located in transmembrane helix six, facing away from the
156 retinal binding pocket (Figures 2a, 2b, see also Baldwin 1993, Hunt et al. 1996). Neither residue
157 100 nor 255 are known to be key spectral tuning sites in *rhodopsin* (Yokoyama 2000), but site-
158 directed mutagenesis experiments to determine the effect of these substitutions on the absorbance
159 spectrum should be conducted in the future. All three of these SNPs possess the exact same F_{ST}
160 and changes in genotype were completely consistent across all samples, suggesting that these
161 sites are tightly linked.

162 The most strongly segregating SNP ($F_{ST} = 0.88$) occurred at amino acid residue 261 of
163 *rhodopsin*, which is located in transmembrane helix six, facing the retinal binding pocket of the
164 protein (Figures 2a, 2b, see also Baldwin 1993, Hunt et al. 1996, Yokoyama 2000). *Coregonus*
165 *artedi*, *C. hoyi*, and *C. zenithicus*, inhabitants of a red-shifted light environment, were primarily
166 homozygous for tyrosine (Figure 3). This amino acid substitution is known to cause an 8 nm red-

167 shift in the absorbance spectrum (Yokoyama et al. 1995). Meanwhile, *C. kiyi*, which inhabits the
168 blue-shifted deeper waters of Lake Superior, was completely homozygous for phenylalanine,
169 which does not produce a similar red-shift in photic absorbance (Figure 3; Yokoyama et al.
170 1995). Genotypic associations at this locus vary consistently across the depth gradient (Figure 3),
171 providing evidence that *C. kiyi* is adapted to life in deep water after evolving from shallow-water
172 ancestors. This hypothesis is further corroborated by phenotypic data, as *C. kiyi* have
173 significantly larger eye diameters (as a proportion of total head length) than *C. artedi* ($p <$
174 0.001), *C. zenithicus* ($p < 0.001$), and *C. hoyi* ($p < 0.001$), consistent with Eshenroder et al.
175 (2016) (Figure S1). The predictable variation of both genetic and morphological traits along the
176 axis of the depth gradient provides key evidence that local adaptation by depth accompanies
177 diversification of Lake Superior ciscoes (Figure S2).

178 Hill et al. (2019) examined the shift between the two aforementioned amino acids at
179 *rhodopsin* residue 261 in a deep phylogenetic context, suggesting that many lineages, including
180 salmonids, are likely derived from a marine ancestor possessing the allele encoding the blue-
181 shift-associated 261Phe. Additionally, Hill et al. (2019) found that fish lineages which have
182 undergone a habitat change from blue-shifted marine waters to red-shifted brackish or freshwater
183 have independently converged on the red-shift-associated 261Tyr phenotype over 20 times
184 across the fish tree of life. Here, we show that the exact same substitution has occurred in Great
185 Lakes ciscoes, as the 261Tyr phenotype is predominant among *Coregonus artedi*, *C. hoyi*, and *C.*
186 *zenithicus*, which inhabit the red-shifted shallow water of Lake Superior. This finding supports
187 the hypothesis that local adaptation to a novel visual environment is driving parallel molecular
188 evolution across the fish tree of life. Interestingly, it appears that deep-water *C. kiyi* has
189 undergone a reversal to the blue-shifted marine ancestral state (261Phe) after more than 100

190 million years indicating that *rhodopsin* residue 261 may be able to “toggle” (*sensu* Delport et al.
191 [2008]) between these two amino acids depending on what is advantageous in a particular photic
192 environment, even across incredibly long time scales.

193 **Conclusions:**

194 The present study provides evidence of the utility of the Oxford Nanopore Flongle device
195 for genotyping complex eukaryotic samples by long-read amplicon sequencing. The protocol
196 described is simple and reliable, and offers the promise of rapid, low-cost genotyping in non-
197 model organisms. This methodology was employed here to understand the genetic basis of local
198 adaptation and ecological differentiation among Great Lakes ciscoes.

199 The results of this study indicate that local adaptation to distinct visual environments is
200 associated with genetic and morphological differentiation among the closely related ciscoes of
201 the Great Lakes. The identification of several high F_{ST} SNPs in *rhodopsin*, including Phe261Tyr,
202 is particularly relevant, as the shifts between these two amino acids at residue 261 are identical to
203 those observed across similar depth gradients in phylogenetically-distant fishes (Hill et al. 2019).
204 This result suggests that evolutionary parallelism via single-nucleotide changes at this site is
205 driving phenotypic convergence of distantly related groups exposed to similar photic
206 environments. Additionally, the discovery of a reversal to the ancient ancestral state in *C. kiyi* at
207 this site provides evidence of genetic toggling, whereby organisms may be able to transition bi-
208 directionally between different states at this site in response to environmental pressures. This
209 result is striking because the genetic background is presumably very different across these taxa
210 after more than 100 million years of divergence. In addition, the potential for epistatic
211 interactions is expected to be increased across such deep phylogenetic splits, further reducing the
212 likelihood of parallel evolution (Storz 2016). The observation of amino acid toggling in Great

213 Lakes *Coregonus* species stands in stark contrast to the general prediction that evolution can only
214 reverse itself after short time periods (Storz 2016; Blount et al. 2018).

215

216 **Acknowledgements**

217 We thank the U.S. Geological Survey Research Vessel Kiyi Captain Joe Walters, First Mate
218 Keith Peterson, and Engineer Charles Carrier, as well as Dan Yule, Mark Vinson, Lori Evrard,
219 Anders Nyman, and the USGS Lake Superior Biological Station and Ontario Ministry of Natural
220 Resources and Forestry for assistance with sample collection. Jessie Pelosi provided critical
221 assistance with data analysis. Mary Alice Coffroth, Tianying Lan, Wendylee Stott, Andrew
222 Muir, Thomas Dowling, Hannah Waterman, Victor Albert, Vincent Lynch, and Omer Gokcumen
223 provided valuable assistance or feedback on the study. Jessica Poulin coordinated the University
224 at Buffalo Honors Program in Biological Sciences that facilitated this research. This work was
225 supported by the Great Lakes Fishery Commission (Award #2018_KRA_44073 to TJK), the
226 University at Buffalo Department of Biological Sciences (Philip G. Miles Fellowship to KME),
227 and the University at Buffalo Honors College (Award to KME).

228 **References:**

229 Ackiss AS, Larson WA, Stott W. 2020. Genotyping-by-sequencing illuminates high levels of
230 divergence among sympatric forms of coregonines in the Laurentian Great Lakes. Evolutionary
231 Applications. 13(5): 1037-1054.

232 Baldwin JM. 1993. The probable arrangement of the helices in G protein-coupled receptors.
233 EMBO J. 12(4): 1693-1703.

234 Cornelis S, Gansemans Y, Deleye L, Deforce D, Van Nieuwerburgh F. 2017. Forensic SNP
235 genotyping using Nanopore MinION sequencing. *Scientific Reports*. 7: 41759.

236 Cornelis S, Gansemans Y, Vander Plaetsen AS, Weymaere J, Willems S, Deforce D, Van
237 Nieuwerburgh F. 2019. Forensic tri-allelic SNP genotyping using nanopore sequencing. *Forensic
238 Science International: Genetics*. 38: 204-210.

239 Danecek P, Schiffels S, Durbin R. 2014. Multiallelic calling model in bcftools (-m).

240 De-Kayne R, Zoller S, Feulner PGD. 2020. A *de novo* chromosome-level genome assembly of
241 *Coregonus* sp. “*Balchen*”: one representative of the Swiss Alpine whitefish radiation. *Molecular
242 Ecology Resources*. doi:10.1111/1755-0998.13187.

243 Delport W, Scheffler K, Seoighe C. 2008. Frequent toggling between alternative amino acids is
244 driven by selection in HIV-1. *PLoS Pathog*. 4(12): e1000242.

245 Eshenroder RL, Vecsei P, Gorman OT, Yule DL, Pratt TC, Mandrak NE, Bunnell DB, Muir
246 AM. 2016. Ciscoes (*Coregonus*, subgenus *Leucichthys*) of the Laurentian Great Lakes and Lake
247 Nipigon. Great Lakes Fishery Commission.

248 Futuyma D, Kirkpatrick M. 2017. Evolution, 4th edn. Sunderland, MA: Sinauer.

249 Harrington KA, Hrabik TR, Mensinger AF. 2015. Visual sensitivity of deepwater fishes in Lake
250 Superior. *PLoS One*. 10(2): e0116173.

251 Hill J, Enbody ED, Pettersson ME, Sprehn CG, Bekkevold D, Folkvord A, Laikre L, Kleinau G,
252 Scheerer P, Andersson L. 2019. Recurrent convergent evolution at amino acid residue 261 in fish
253 rhodopsin. *PNAS*. 116(37): 18473-18478.

254 Hunt DM, Fitzgibbon J, Slobodyanyuk SJ, Bowmaker JK. 1996. Spectral tuning and molecular
255 evolution of rod visual pigments in the species flock of cottoid fish in Lake Baikal. *Vision Res.*
256 36(9): 1217-1224.

257 Kelley LA, Mezulis S, Yates CM, Wass MN, Sternberg MJE. 2015. The Phyre2 web portal for
258 protein modeling, prediction, and analysis. *Nature Protocols.* 10: 845-858.

259 Li H. 2010. Mathematical notes on SAMtools algorithms.

260 Li H. 2011. A statistical framework for SNP calling, mutation discovery, association mapping
261 and population genetical parameter estimation from sequencing data. *Bioinformatics.* 27(21):
262 2987-2993.

263 Li H. 2013. Aligning sequence reads, clone sequences and assembly contigs with BWA-MEM.
264 arXiv:1303.3997.

265 Marques DA, Taylor JS, Jones FC, Di Palma F, Kingsley DM, Reimchen TE. 2017. Convergent
266 evolution of SWS2 opsin facilitates adaptive radiation of threespine stickleback into different
267 light environments. *PLoS Biology.* 15(4): e2001627.

268 Moon J, Jang Y, Kim N, Park WB, Park KI, Lee ST, Jung KH, Kim M, Lee SK, Chu K. 2018.
269 Diagnosis of *Haemophilus influenzae* pneumonia by nanopore 16S amplicon sequencing of
270 sputum. *Emerging Infectious Diseases.* 24(10): 1944-1946.

271 Musilova Z, Cortesi F, Matschiner M, Davies WIL, Patel JS, Stieb SM, de Busserolles F,
272 Malstrøm M, Tørresen OK, Brown CJ, et al. 2019. Vision using multiple distinct rod opsins in
273 deep-sea fishes. *Science.* 364(6440): 588-592.

274 Okano T, Kojima D, Fukada Y, Shichida Y, Yoshizawa T. 1992. Primary structures of chicken
275 cone visual pigments: vertebrate rhodopsins have evolved out of cone visual pigments. PNAS.
276 89(13): 5932-5936.

277 Pettersen EF, Goddard TD, Huang CC, Couch GS, Greenblatt DM, Meng EC, Ferrin TE. 2004.
278 UCSF Chimera -- a visualization system for exploratory research and analysis. J Comput Chem.
279 25(13): 1605-1612.

280 Rames E, Macdonald J. 2018. Evaluation of MinION nanopore sequencing for rapid enterovirus
281 genotyping. Virus Research. 252: 8-12.

282 Romero-Herrera AE, Lehmann H, Joysey KA, Friday AE. 1978. On the evolution of myoglobin.
283 Philos. Trans. R. Soc. B. Biol. Sci. 283(995): 61-163.

284 Rosinski CL, Vinson MR, Yule DL. 2020. Niche partitioning among native ciscoes and
285 nonnative rainbow smelt in Lake Superior. Transactions of the American Fisheries Society.
286 149(2): 184-203.

287 Shin J, Lee S, Go MJ, Lee SY, Kim SC, Lee CH, Cho BK. 2016. Analysis of the mouse gut
288 microbiome using full-length 16S rRNA amplicon sequencing. Scientific Reports. 6: 29681.

289 Stewart CB, Schilling JW, Wilson AC. 1987. Adaptive evolution in the stomach lysozymes of
290 foregut fermenters. Nature. 330: 401-404.

291 Storz JF. 2016. Causes of molecular convergence and parallelism in protein evolution. Nature
292 Reviews Genetics. 17: 239-250.

293 Terai Y, Mayer WE, Klein J, Tichy H, Okada N. 2002. The effect of selection on a long
294 wavelength-sensitive (LWS) opsin gene of Lake Victoria cichlid fishes. PNAS. 99(24): 15501-
295 15506.

296 Turgeon J, Bernatchez L. 2003. Reticulate evolution and phenotypic diversity in North American
297 ciscoes, *Coregonus* ssp. (Teleostei: Salmonidae): implications for the conservation of an
298 evolutionary legacy. Conservation Genetics. 4: 67-81.

299 Turgeon J, Reid SM, Bourret A, Pratt TC, Reist JD, Muir AM, Howland KL. 2016.
300 Morphological and genetic variation in Cisco (*Coregonus artedi*) and Shortjaw Cisco (*C.*
301 *zenithicus*): multiple origins of Shortjaw Cisco in inland lakes require a lake-specific
302 conservation approach. Conservation Genetics. 17: 45-56.

303 Weadick CJ, Chang BSW. 2007. Long-wavelength sensitive visual pigments of the guppy
304 (*Poecilia reticulata*): six opsins expressed in a single individual. BMC Evolutionary Biology. 7:
305 S11.

306 Wood TE, Burke JM, Rieseberg LH. 2005. Parallel genotypic adaptation: when evolution repeats
307 itself. Genetica. 123: 157-170.

308 Yokoyama R, Knox BE, Yokoyama S. 1995. Rhodopsin from the fish, *Astyanax*: role of tyrosine
309 261 in the red shift. Investigative Ophthalmology & Visual Science. 36(5): 939-945.

310 Yokoyama S. 2000. Molecular evolution of vertebrate visual pigments. Progress in Retinal and
311 Eye Research. 19(4): 385-419.

312 Zhang J, Kumar S. 1997. Detection of convergent and parallel evolution at the amino acid
313 sequence level. Mol Biol Evol. 14(5): 527-536.

314 **Tables:**

315 **Table 1.** Average coverage and fragment length for the five amplified opsin genes on the Flongle
316 platform.

| Gene name | Average coverage | Fragment length (bp) |
|-------------|------------------|----------------------|
| <i>LWS</i> | 722 | 1879 |
| <i>RH1</i> | 5409 | 763 |
| <i>RH2</i> | 846 | 2079 |
| <i>SWS1</i> | 4734 | 815 |
| <i>SWS2</i> | 4237 | 960 |

317

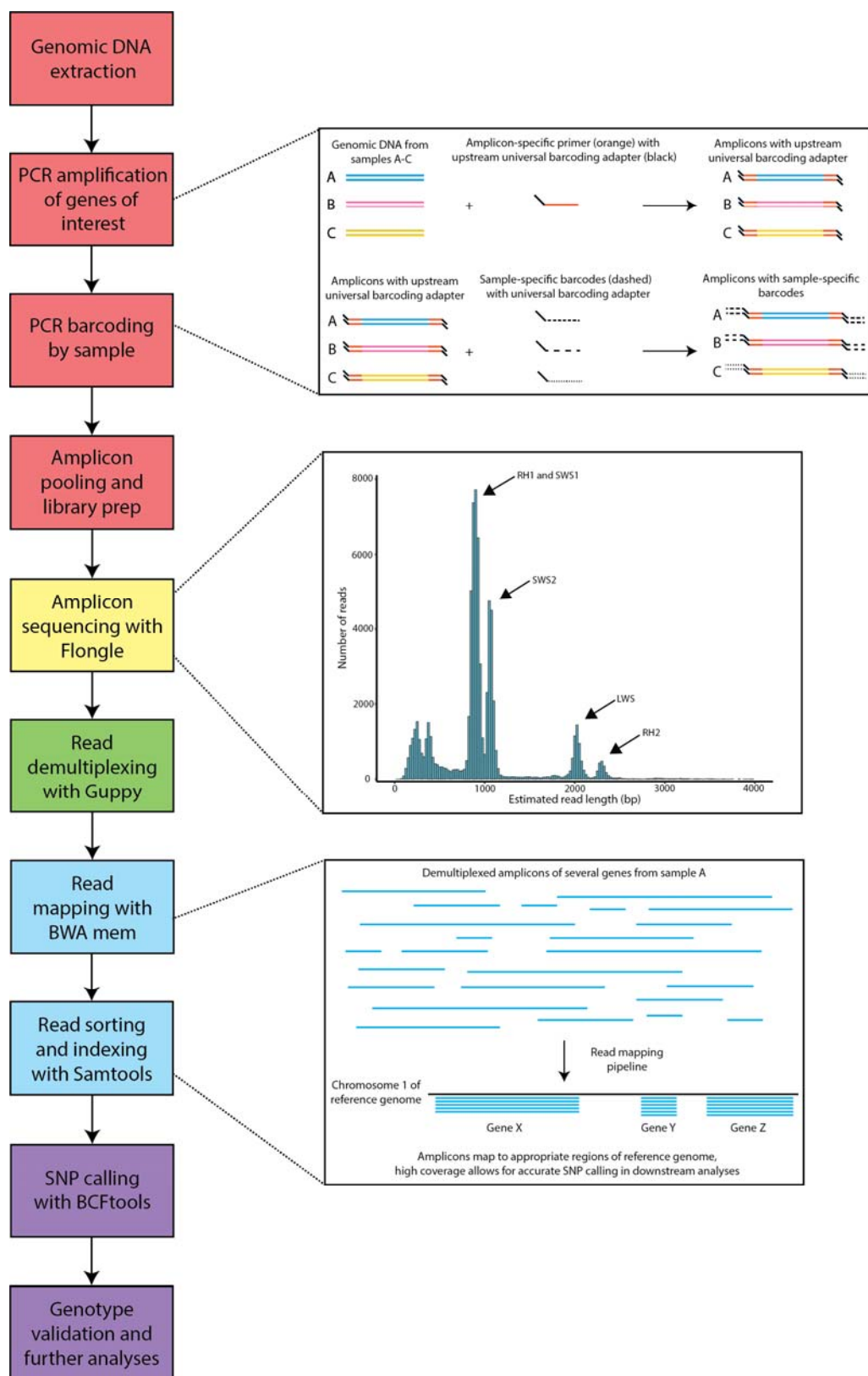
318 **Table 2.** Pairwise Weir-Cockerham F_{ST} estimates across species for all genes (above diagonal)
319 and for *rhodopsin* only (below diagonal).

| Species | <i>C. artedi</i> | <i>C. hoyi</i> | <i>C. kiyi</i> | <i>C. zenithicus</i> |
|----------------------|------------------|----------------|----------------|----------------------|
| <i>C. artedi</i> | - | 0.042 | 0.092 | 0.049 |
| <i>C. hoyi</i> | 0.26 | - | 0.056 | 0.005 |
| <i>C. kiyi</i> | 0.68 | 0.34 | - | 0.068 |
| <i>C. zenithicus</i> | 0.26 | 0 | 0.34 | - |

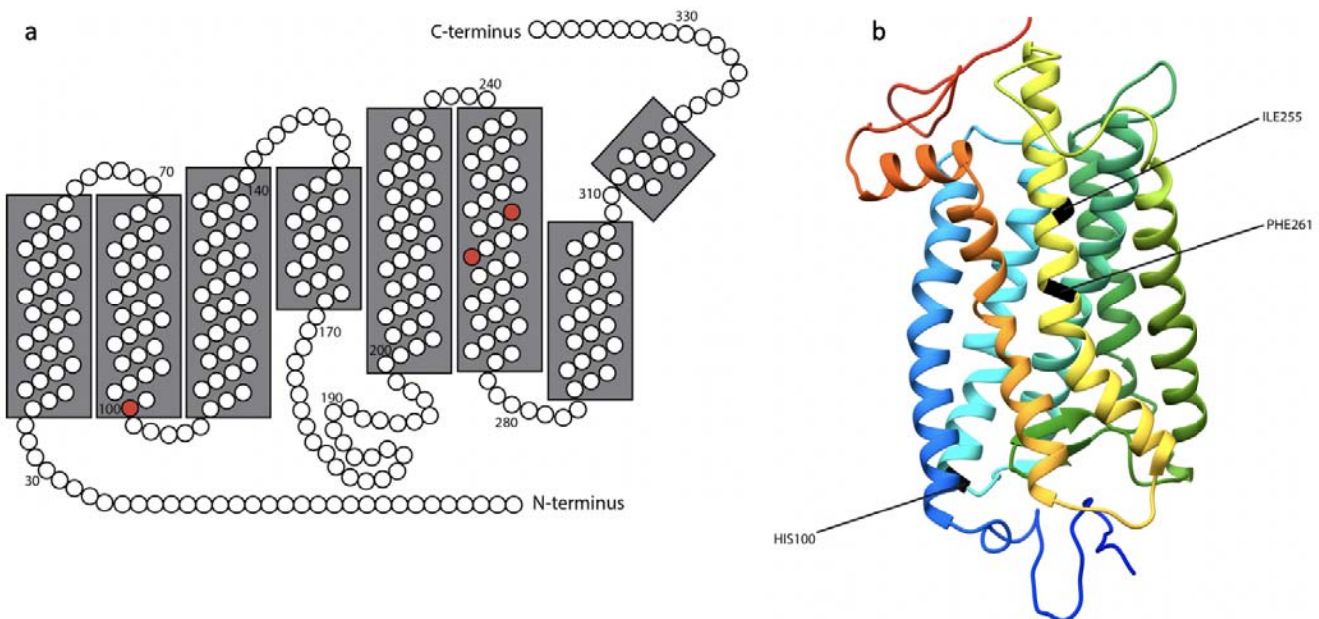
320

321

322 **Figures:**



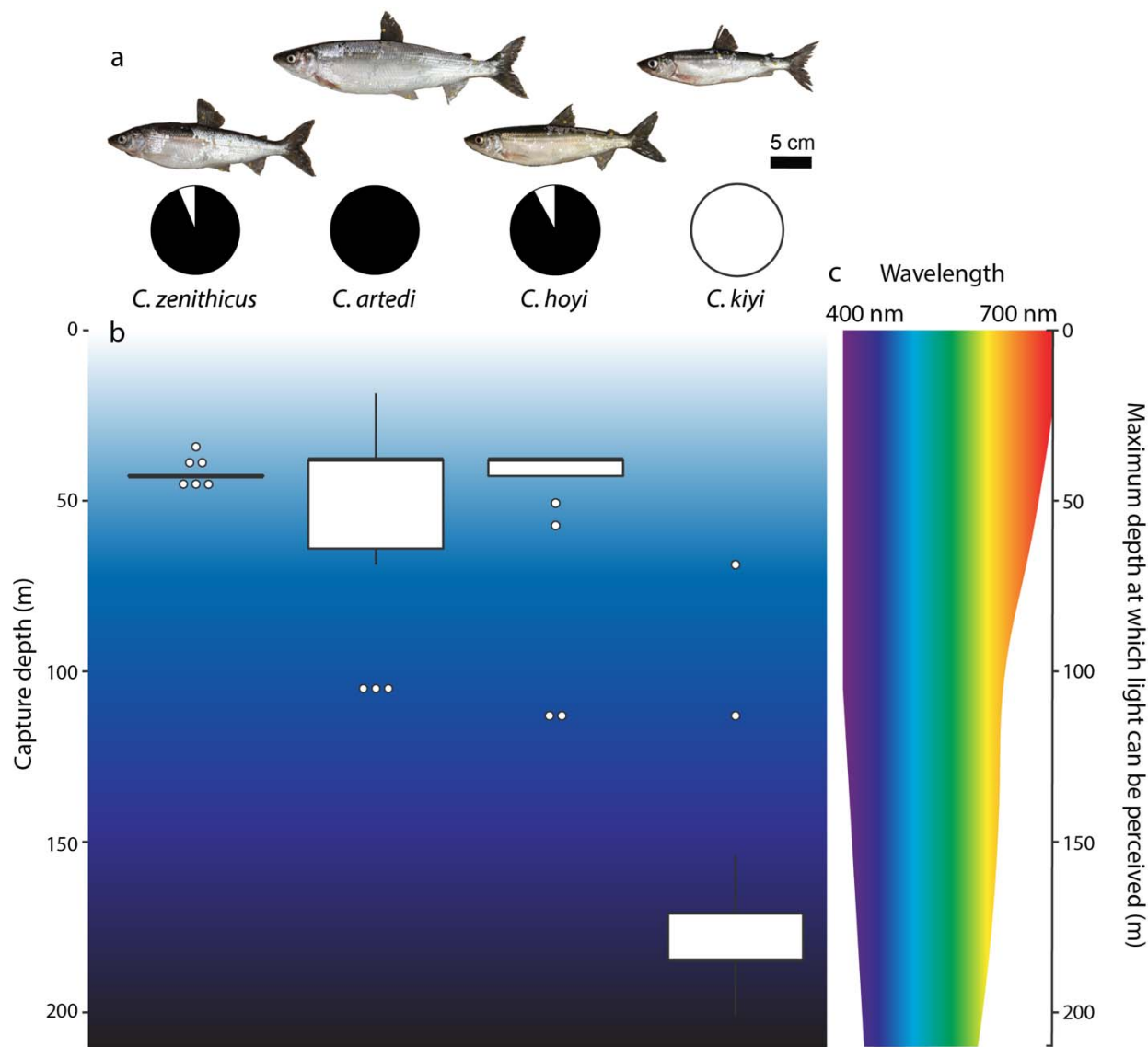
324 **Figure 1.** Summary of steps for amplicon sequencing and bioinformatic analyses. Boxes on the
325 left represent individual steps, color-coded based on their phase: red represents sample
326 preparation, yellow represents nanopore sequencing, green represents sample demultiplexing,
327 blue represents read mapping, and purple represents genotyping and analysis. Larger boxes to the
328 right show additional information for each of the steps: the simplified mechanisms by which
329 amplicons are generated and barcoded (top); frequency histogram with read length on the x-axis
330 and number of reads in the y-axis (middle); and how reads are mapped to the reference genome
331 (bottom).



332

333 **Figure 2.** a) 2-D model of *Coregonus artedi* rhodopsin based on a 3-D model generated using
334 PHYRE v2.0 (Kelley et al. 2015) and visualized in UCSF Chimera (Pettersen et al. 2004).
335 Amino acid residues are numbered in order from N-terminus to C-terminus, and amino acid
336 residues 100, 255, and 261 are colored in red. 2-D model was constructed for the specific model
337 obtained for *Coregonus artedi*, following Yokoyama (2000) and Musilova et al. (2019). b) 3-D
338 model of bovine rhodopsin, colored blue (N-terminus) to red (C-terminus). Amino acid residues
339 100, 255, and 261 have been colored in black, and are labeled accordingly.

340



342 **Figure 3.** a) The four cisco species included in this study: *Coregonus zenithicus*, *C. artedi*, *C.*
343 *hoyi*, and *C. kiyi* (left → right). Pie charts below each photo indicate the allele frequency at
344 residue 261 of *rhodopsin*, where black represents the allele coding for tyrosine and white
345 represents the allele coding for phenylalanine. b) Boxplots indicating the approximate capture
346 depths of samples from each of the four species. c) Visible light spectrum, from approximately
347 400-700 nm wavelength. The narrowing of the spectrum with increased depth shows how the

348 ability of organisms to perceive certain wavelengths of light diminishes with increasing depth,

349 particularly with red and orange light (following Harrington et al. 2015).